Supplement of Atmos. Chem. Phys., 25, 3011–3028, 2025
https://doi.org/10.5194/acp-25-3011-2025-supplement

Atmospheric Chemistry and Physics
Open Access
EGU

Supplement of

Accurate elucidation of oxidation under heavy ozone pollution: a full suite of radical measurements in the chemically complex atmosphere

Renzhi Hu et al.

Correspondence to: Guoxian Zhang (gxzhang@aiofm.ac.cn) and Pinhua Xie (phxie@aiofm.ac.cn)

Supplements

Figures in supplementary material

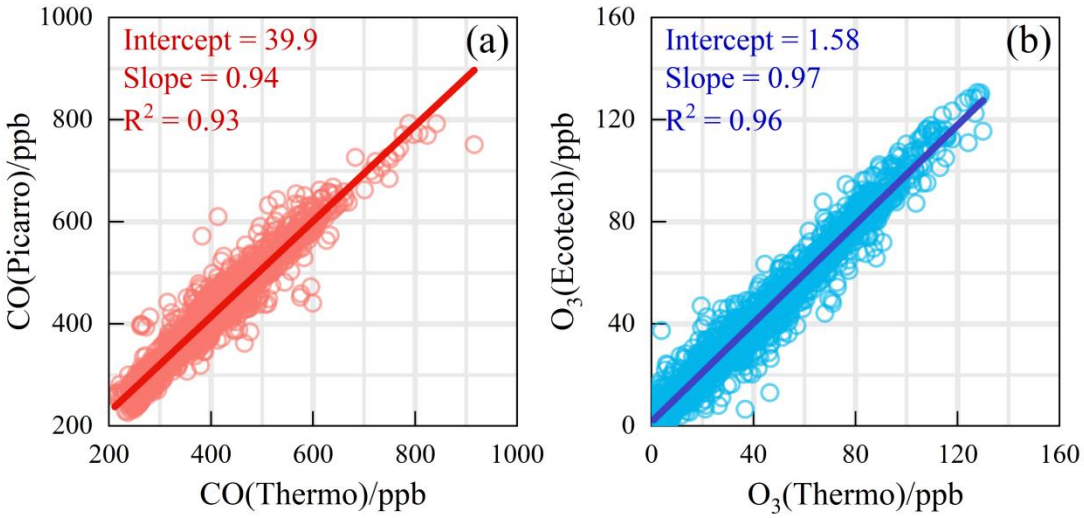

Fig. S1. The comparison results between different technologies. **(a)** CO measurements by Thermo 48i and Picarro-G2401. **(b)** O_3 measurements by Thermo 49i and Ecotech EC9810B.

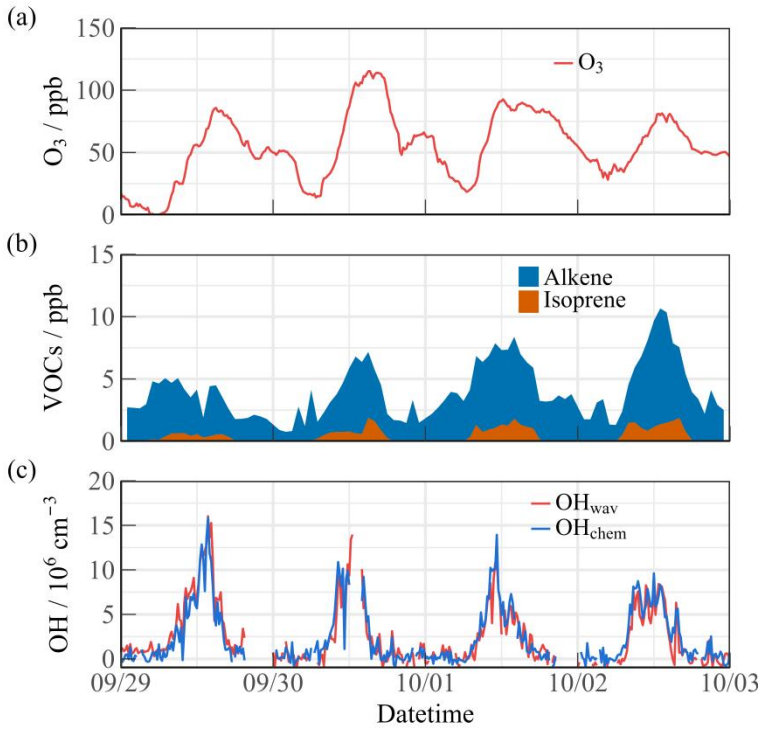

Fig. S2. Results of an additional atmospheric oxidation observation experiment in the same location and season in 2022. **(a)** Ozone concentration **(b)** Concentrations of alkene and isoprene, respectively. **(c)** The OH concentrations achieved by chemical modulation (OH_{chem}) and wavelength modulation (OH_{wav}).

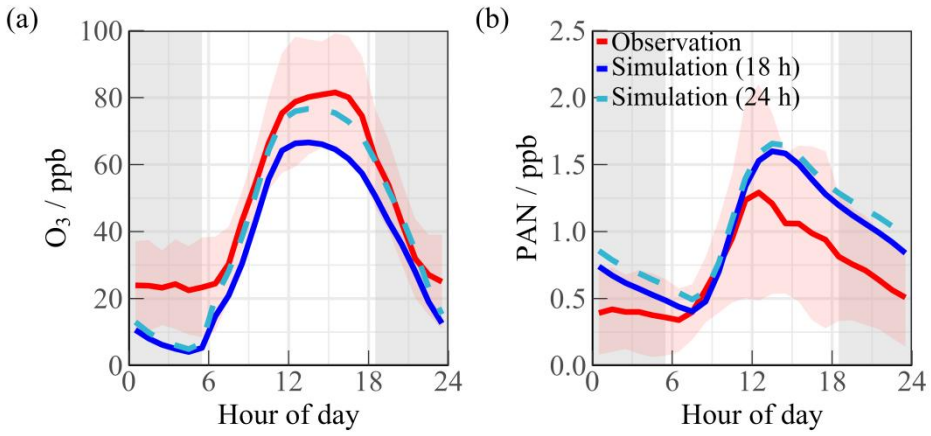

Fig. S3. The comparison results of **(a)** ozone and **(b)** PAN between simulation and observation. The red line represents the observed concentrations, while the blue and green lines represent the simulation results based on the RACM2-LIM1 mechanism for deposition times of 18 and 24 hours, respectively.

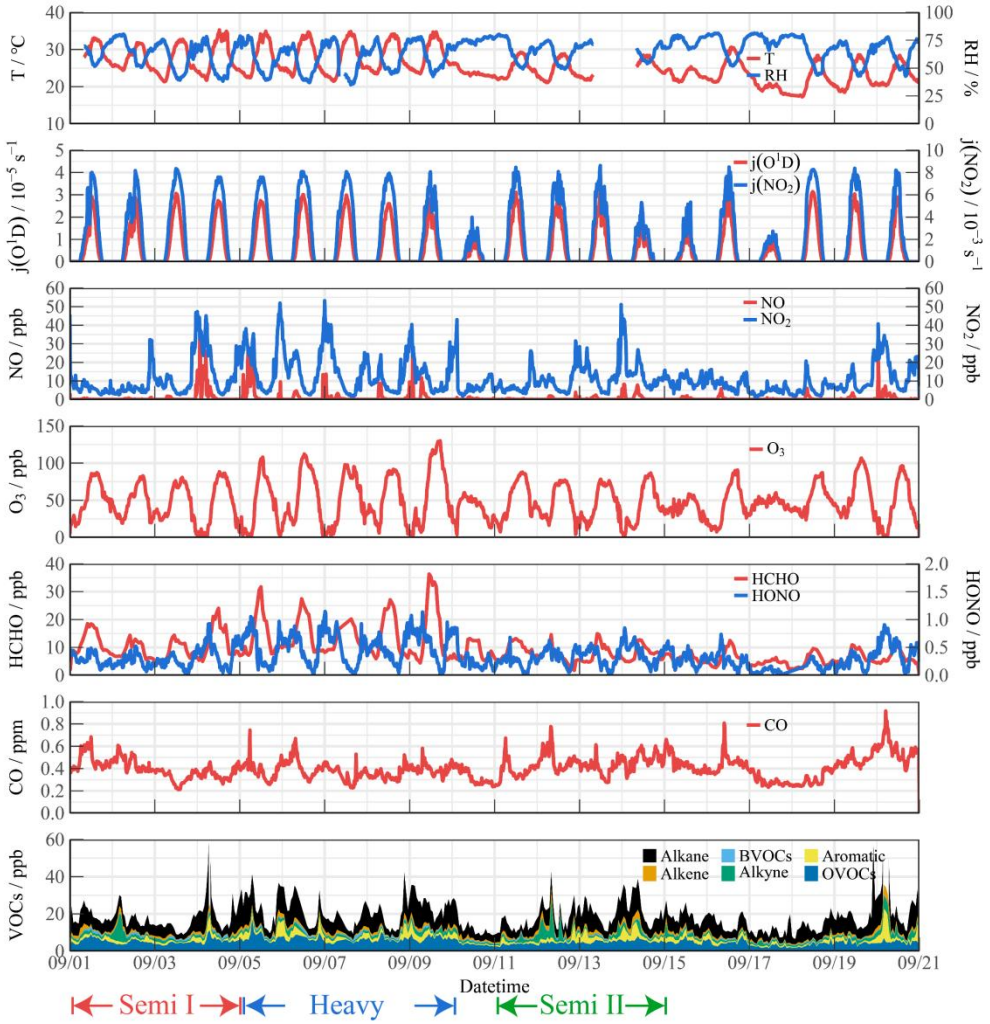

Fig. S4. Time series of observed meteorological and chemical parameters during the campaign. The entire ozone pollution is divided into three continuous periods according to pollution level (Semi I, Heavy, and Semi II).

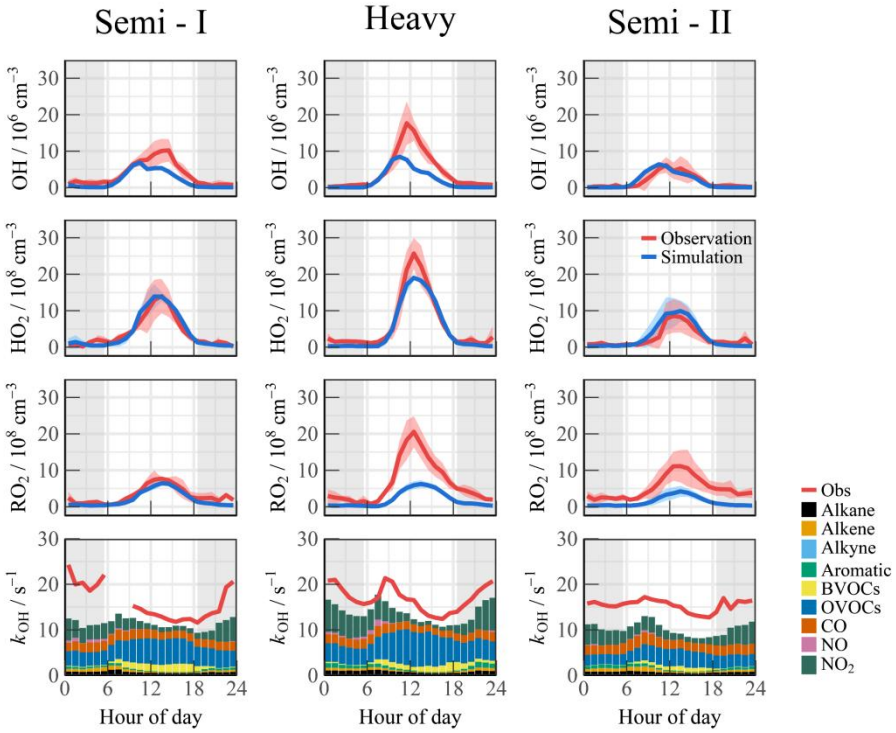

Fig. S5. Diurnal profiles of the observed and modelled OH, HO_2, RO_2 and k_{OH} in different episodes (Semi I, Heavy, and Semi II). The simulation results are output by the RACM2-LIM1 mechanism. The coloured shadows denote the 25 and 75% percentiles. The grey areas denote nighttime.

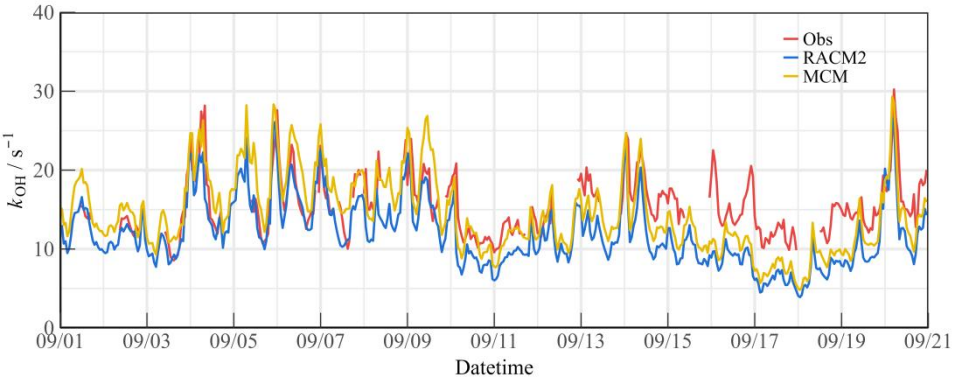

Fig. S6. Timeseries of the observed and modelled k_{OH} during the observation period.

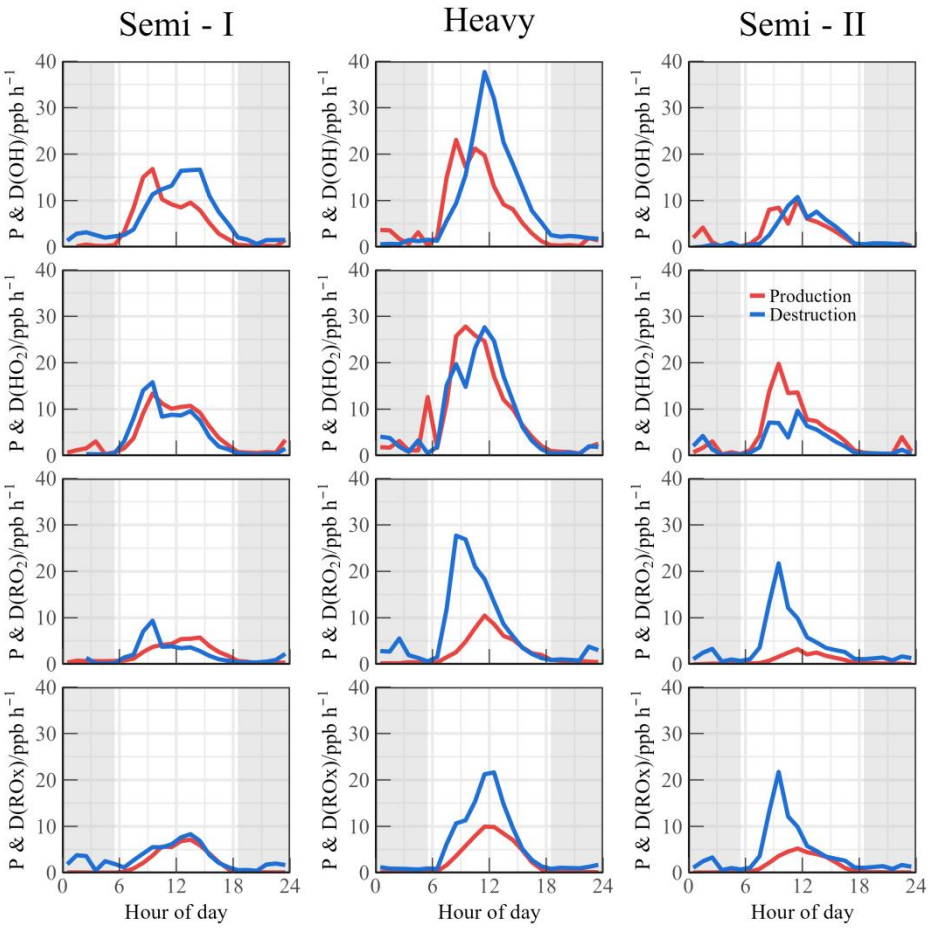

Fig. S7. Experimental budget for OH, HO_2, RO_2 and total ROx radicals during different periods.

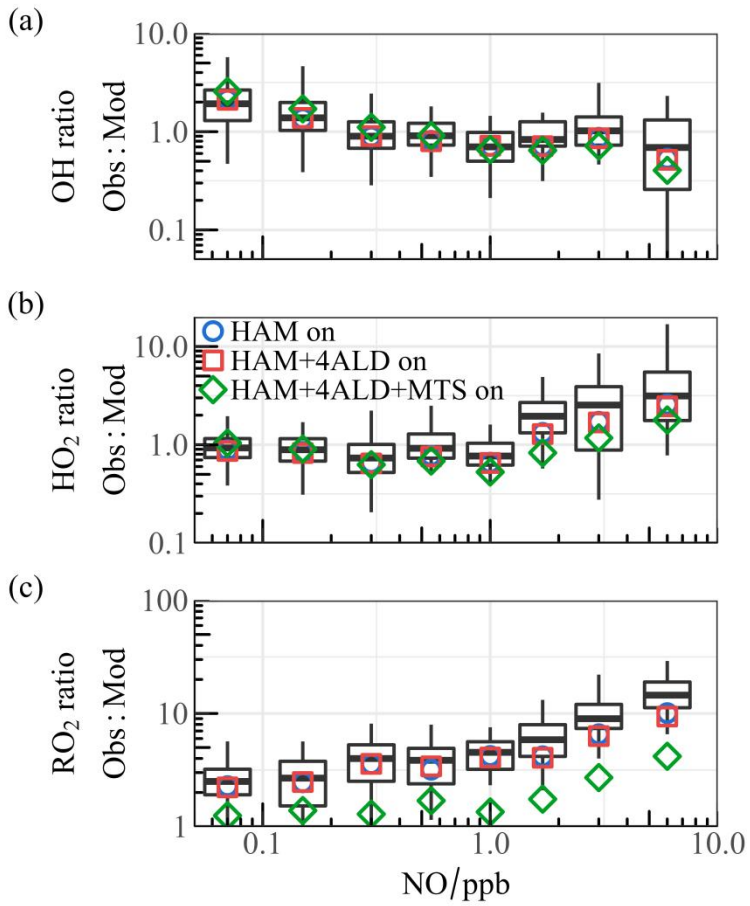

Fig. S8. The relationship between NO and the "observation-to-simulation" ratios for **(a)** OH, **(b)** HO_2, and **(c)** RO_2 concentrations. Boxplot diagrams illustrate the dataset's minimum, 25th percentile, median, 75th percentile, and maximum values. The point styles (circular, square, diamond-shaped) represent the median values for the base model as well as for different mechanisms added to the model within various ranges.

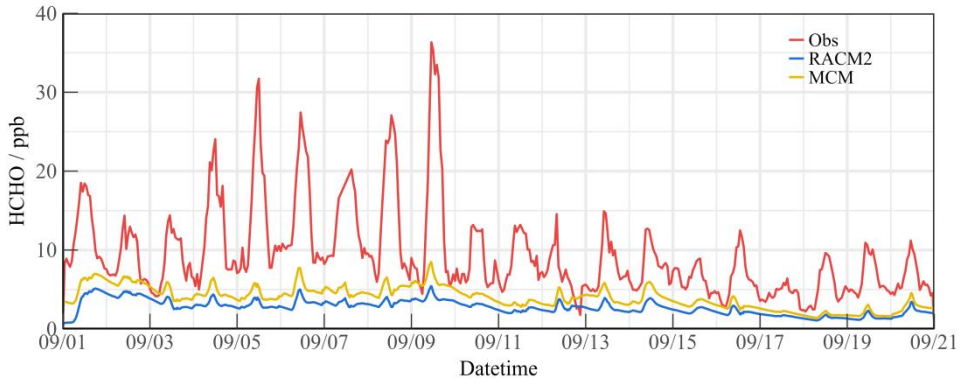

Fig. S9. The observed and modeled HCHO concentration during the TROPSTECT-YRD campaign.

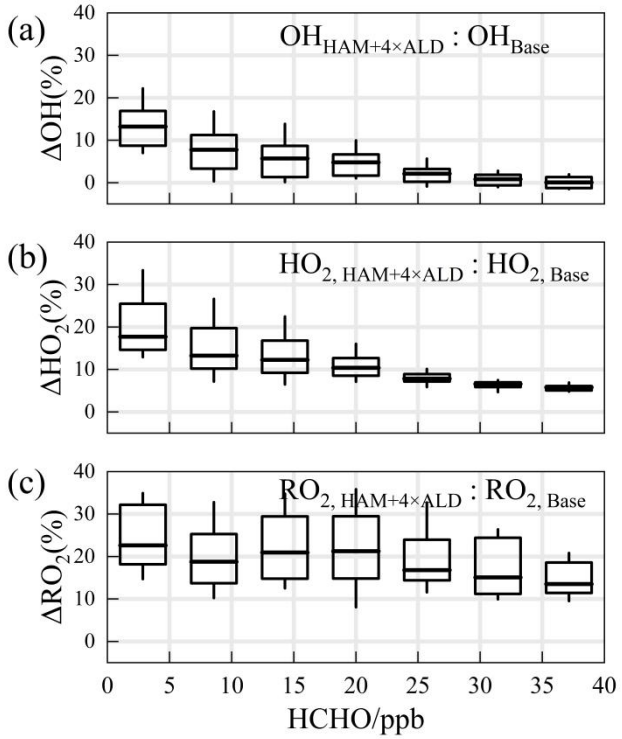

Fig. S10. The relationship between the differences in the simulation of **(a)** OH, **(b)** HO_2, and **(c)** RO_2 radical concentrations by HAM mechanism and the base scenario across the entire photochemical spectrum. An empirical hypothesis is proposed to amplify the concentration of higher-order aldehydes by a factor of about 4, which is the proportion of formaldehyde concentration underestimated by the model. The boxplots represent the 10%, 25%, median, 75%, and 90% of the data, respectively.

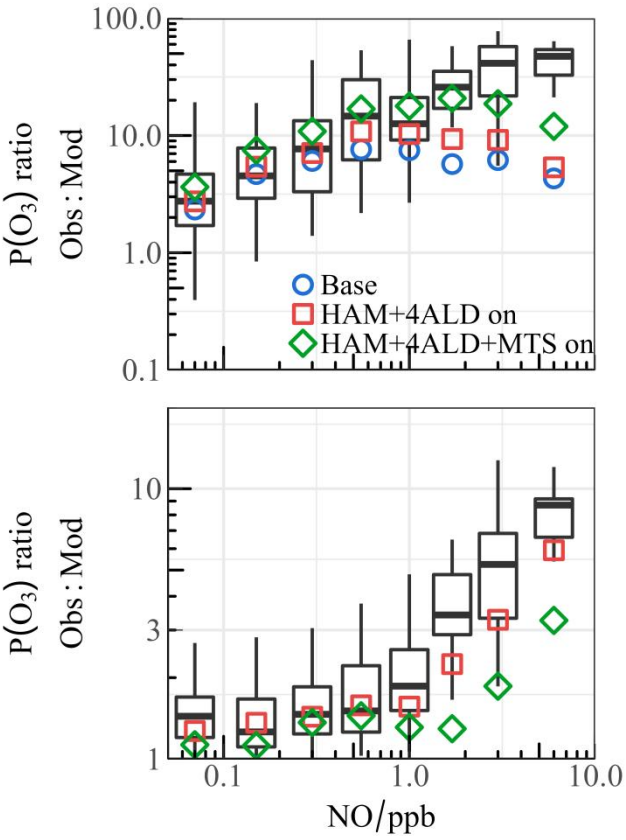

Fig. S11. The relationship between NO and **(a)** P(Ox), **(b)** P(Ox) (Obs:Mod). Boxplot diagrams are used to

illustrate the minimum, 25th percentile, median, 75th percentile, and maximum values of the observed dataset. The point styles (circular, square, diamond-shaped) represent the median values for the base model as well as for different mechanisms added to the model within various ranges.

Tables in supplementary material

Table.S1. Detailed information of supporting measurements.

Species	Methods	limit of detection	Accuracy (1 σ)	Time resolution
OH	LIF	3.3×10^5 cm^{-3}	±13%	60s
HO_2	LIF	1.1×10^6 cm^{-3}	±17%	60s
RO_2	LIF	2.6×10^6 cm^{-3}	±21%	60s
k_{OH}	LP-LIF	0.3 s^{-1}	±20%	180s
Temperature	Met One 083E	−50 to 50 °C	±0.5%	60s
Relative humidity	Met One 083E	0 − 100%	±2.0%	60s
WS	Met One 014A	0.45 − 60 m/s	± 0.11 m/s	1min
WD	Met One 024A	0−360° (>0.45 m/s)	±5°	1min
Pressure	Met One 092	600−1100 hPa	±0.5%	60s
J-values	SR	-	± 10%	60s
$PM_{2.5}$	TEOM	0.1 μg/m^3	± 10%	1h
O_3	UV	0.5 ppb	±10%	60s
	UV	0.4 ppb	±10%	60s
NO	CL	50 ppt	±10%	60s
NO_2	CL	50 ppt	±10%	60s
SO_2	UV-F	0.1 ppb	±10%	60s
CO	NDIR	50 ppb	±10%	60s
	CRDS	15 ppb	±10%	60s
PAN	GC-ECD	50 ppt	±10%	60s
HONO	CEAS	150 ppt	±15%	60s
HCHO	Hantzsch	200 ppt	±5%	60s
NMHCs	GC-MS/FID	5−70 ppt	± 10−15%	1h

Table S2. Information table for parts of the VOC monitoring species by online GC-MS/FID. Revised by (Zhu et al., 2021).

Name	Molecular formula	m/z	MIR	Uncertainty	LOD
MTBE	$C_5H_{12}O$	88.15	0.73	3.3%	0.012
Ethane	C_2H_6	30.07	0.28	4.6%	0.013
Propane	C_3H_8	44.10	0.49	0.9%	0.010
n-Butane	C_4H_{10}	58.12	1.15	0.3%	0.012
Isobutane	C_4H_{10}	58.12	1.23	0.6%	0.008
Isopentane	C_5H_{12}	72.15	1.45	0.7%	0.008
n-Pentane	C_5H_{12}	72.15	1.31	1.5%	0.008
Cyclohexane	C_6H_{12}	84.16	1.25	1.5%	0.013
n-Hexane	C_6H_{14}	86.18	1.24	2.0%	0.006
2-Methylpentane	C_6H_{14}	86.18	1.5	3.8%	0.009
3-Methylpentane	C_6H_{14}	86.18	1.8	1.9%	0.009
Ethylene	C_2H_4	28.05	9	1.5%	0.013
Propene	C_3H_6	42.08	11.66	1.0%	0.010
Acetylene	C_2H_2	26.04	0.95	1.3%	0.018
Chloromethane	CH_3Cl	50.49	0.038	9.1%	0.011
Dichloromethane	CH_2Cl_2	84.93	0.041	3.2%	0.001
1,2-Dichloroethane	$C_2H_4Cl_2$	98.96	0.21	3.4%	0.001
1,2-Dichloropropane	$C_3H_6Cl_2$	112.99	0.29	1.1%	0.012
Chloroform	$CHCl_3$	119.38	0.022	1.2%	0.007
Freon-11	CCl_3F	137.40	/	4.6%	0.010
1,3-Dichlorobenzene	$C_6H_4Cl_2$	147.00	/	9.6%	0.022
Tetrachloromethane	CCl_4	153.82	0	1.5%	0.003
Freon-113	$C_2Cl_3F_3$	187.38	/	2.7%	0.004

Table.S3. The comprehensive list of model constraints.

Categories	Species
Meteorology	Temperature, Relative humidity, Pressure, Jvalues
Trace gases	O_3, NO, NO_2, SO_2, CO, PAN, HONO
Alkanes	methane, ethane, propane, n-butane, isobutane, cyclopentane, n-pentane, isopentane, cyclohexane, methyl cyclopentane, 2,3-dimethyl butane, 2,2-dimethyl butane, n-hexane, 2-methyl pentane, 3-methyl pentane, methyl cyclohexane, n-heptane, 2-methyl hexane, 2,3-dimethyl pentane, 2,4-dimethyl pentane, 3-methyl hexane, n-octane, 2,3,4-trimethyl pentane, 2-methyl heptane, 3-methyl heptane, 2,2,4-trimethyl pentane, n-nonane, n-decane, n-undecane, n-dodecane
Alkenes	ethene, propene, 1,3-butadiene, 1-butene, cis-2-butene, trans-2-butene, 1-pentene, cis-2-pentene, trans-2-pentene, 1-hexene, styrene
BVOCs	isoprene
Alkynes	acetylene
Aromatics	benzene, toluene,ethyl benzene, o-xylene, m-xylene, n-propyl benzene, isopropyl benzene, p-ethyl toluene, o-ethyl toluene, m-ethyl toluene, 1,2,4-trimethyl benzene, 1,3,5-trimethyl benzene, 1,2,3-trimethyl benzene, p-diethyl benzene, m-diethyl benzene
OVOCs	HCHO, acetaldehyde, MACR, MVK

Table.S4. Gas-phase kinetics for the monoterpene species in RACM2 mechanism. API and LIM stand for α-pinene and limonene, respectively; APIP and LIMP represents peroxy radicals derived from API and LIM, respectively; ETHP refers to peroxy radicals generated from ethane; KETP denotes peroxy radicals formed from ketones; ALD signifies C_3 and higher aldehydes; KET indicates ketones; OLNN pertains to the NO_3-alkene adduct that reacts to form carbonitrates and HO_2; OLND pertains to the NO_3-alkene adduct that reacts through decomposition; ACT signifies acetone; ORA1 denotes formic acid; ONIT represents organic nitrate; OP2 denotes higher organic peroxides; MO2 signifies methyl peroxy radical; MOH indicates methanol; ROH denotes C3 and higher alcohols; ACO3 represents acetyl peroxy radicals; ORA2 denotes acetic acid and other higher acids.

Reaction	Reaction rate constant (cm^3s^{-1})
API + OH → APIP	$1.21 \times 10^{-11}\exp(440/T)$
API + O_3 → 0.85 × OH + 0.1 × HO_2 + 0.2 × ETHP + 0.42 × KETP + 0.14 × CO + 0.02 × H_2O_2 + 0.65 × ALD + 0.53 × KET	$5.0 \times 10^{-16}\exp(-530/T)$
API + NO_3 → 0.1 × OLNN + 0.9 × OLND	$1.19 \times 10^{-12}\exp(490/T)$
APIP + NO → 0.82 × HO_2 + 0.82 × NO_2 + 0.23 × HCHO + 0.43 × ALD + 0.44 × KET + 0.07 × ORA1 + 0.18 × ONIT	4.0×10^{-12}
APIP + HO_2 → OP2	1.5×10^{-11}
APIP + MO_2 → HO_2 + 0.75 × HCHO + 0.75 × ALD + 0.75 × KET + 0.25 × MOH + 0.25 × ROH	$3.56 \times 10^{-14}\exp(708/T)$
APIP + ACO_3 → 0.5 × HO_2 + 0.5 × MO_2 + ALD + KET + ORA2	$7.4 \times 10^{-13}\exp(765/T)$
APIP + NO_3 → HO_2 + NO_2 + ALD + KET	1.2×10^{-12}
LIM + OH-->LIMP	$4.2 \times 10^{-11}\exp(401/T)$
LIM + O_3-->0.85 × HO + 0.1 × HO_2 + 0.16 × ETHP + 0.42 × KETP + 0.02 × H_2O_2 + 0.14 × CO + 0.46 × OLT + 0.04 × HCHO + 0.79 × MACR + 0.01 × ORA1 + 0.07 × ORA2	$2.95 \times 10^{-15}\exp(-783/T)$
LIM + NO_3-->0.71 × OLNN+0.29 × OLND	1.22×10^{-11}
LIMP + NO-->HO_2 + NO_2 + 0.05 × OLI + 0.43 × HCHO + 0.68 × UALD + 0.07 × ORA1	4.0×10^{-12}
LIMP + HO_2-->OP_2	1.5×10^{-11}

LIMP + MO_2-->HO_2 + 0.192 × OLI + 1.04 × HCHO + 0.308 × MACR + 0.25 × MOH + 0.25 × ROH	$3.56 \times 10^{-14}\exp(708/T)$
LIMP + ACO_3-->0.5 × HO_2 + 0.5 × MO_2 + 0.192 × OLI + 0.385 × HCHO + 0.308 × MACR + 0.5 × ORA2	$7.4 \times 10^{-13}\exp(765/T)$
LIMP + NO_3-->HO_2 + NO_2 + 0.385 × OLI + 0.385 × HCHO + 0.615 × MACR	1.2×10^{-12}

Table.S5. The reactions and reaction rate constants of the higher aldehyde autoxidation mechanism. Revised by (Yang et al., 2024). ACO_3 and HKET denote acetyl peroxy radicals and hydroxy ketone, respectively. j(MACR) represents the photolysis rate constant of methacrolein (MACR). Ten times MACR photolysis frequency order of about 10^4 s^{-1}, which is the base case setup of HPC photolysis rate used in the HAM.

Reaction	**Reaction rate constant**
$R(CO)O_2$ → ·OOR(CO)OOH	0.321 s^{-1}
·OOR(CO)OOH + NO → ·OR(CO)OOH + NO_2	8.7×10^{-12} cm^3s^{-1}
·OR(CO)OOH → HOR(CO)OO·	1.15×10^6 s^{-1}
HOR(CO)OO· → HOR(CO)OOH	0.9 s^{-1}
HOR(CO)OOH → HO_2 + HPC	10^4 s^{-1}
HPC + *hv* → OH + ACO_3 + HKET	10 × j(MACR)

References

Yang, X., Wang, H., Lu, K., Ma, X., Tan, Z., Long, B., Chen, X., Li, C., Zhai, T., Li, Y., Qu, K., Xia, Y., Zhang, Y., Li, X., Chen, S., Dong, H., Zeng, L., and Zhang, Y.: Reactive aldehyde chemistry explains the missing source of hydroxyl radicals, Nat Commun, 15, 1648, 10.1038/s41467-024-45885-w, 2024.

Zhu, B., Huang, X.-F., Xia, S.-Y., Lin, L.-L., Cheng, Y., and He, L.-Y.: Biomass-burning emissions could significantly enhance the atmospheric oxidizing capacity in continental air pollution, Environ. Pollut., 285, 10.1016/j.envpol.2021.117523, 2021.